

# An optimized upper divertor with divertor-coils to study enhanced divertor configurations in ASDEX Upgrade

A. Herrmann, M. Teschke, I. Zammuto, M. Faitsch, A. Kallenbach, K. Lackner, T. Lunt, R. Neu, M. Rott, G. Schall, B. Sieglin, S. Vorbrugg, M. Weissgerber, M. Wischmeier, H. Zohm, and the ASDEX Upgrade team

*Max-Planck-Institut für Plasmaphysik, D-85748 Garching, Germany*

A new upper divertor with in-vessel coils to investigate ‘advanced’ magnetic configurations will be installed in ASDEX Upgrade. ‘Advanced’ magnetic configurations are part of a risk mitigation strategy should the conventional divertor configuration approach not be applicable for future fusion reactors. The concept of the new upper divertor, Div-IIo, consists of an outer divertor with embedded divertor coils, an inner divertor and a cryo pump with  $15 \text{ m}^3/\text{s}$  effective pumping speed in the private flux region. The new divertor coils will be designed for 50 kAt and can be operated with 5 s plateau phase. This paper presents the design concept of the divertor and coil support structure, the coils and the cryo pump. In addition the forces to the divertor structure due to normal operation and during disruptions are discussed.

Keywords: ASDEX Upgrade, Divertor, Tungsten, Diagnostics, Manipulator

## 1. Introduction

ASDEX Upgrade (AUG) came into operation in 1991. It was designed as a tokamak with reactor relevant shaping. The coil and control system allows to operate in lower single null (LSN), double null (DN) or upper single null (USN) with up to 1.6 MA plasma current and an initially open divertor configuration [1]. Divertor enhancements were concentrated on the lower divertor that was finally transferred to a solid tungsten divertor with vertical target plates and a large flexibility for magnetic configurations. Consequently, the physics program of AUG is concentrated on LSN magnetic configurations using this optimized lower divertor.

The controlled exhaust of power and particles from magnetically confined fusion plasma has been identified as one of the critical issues for the success of future fusion power plants. Advanced divertor geometries such as the Snowflake and Super-X configurations are alternatives to the conventional single null divertor configuration with solid W-targets as foreseen for ITER. The investigation of such ‘advanced’ divertor configurations is part of a risk mitigation strategy should the conventional divertor configuration approach turn out not to be applicable to a future fusion reactor.

The extension of the AUG physics program towards the investigation of advanced divertor configurations requires a new divertor design, the installation of in-vessel coils and of a cryo pump. This modification will be done in the upper divertor, keeping the flexibility and the elaborate diagnostics for physics investigation in the lower divertor as in the past.

The conceptual design for the upper divertor structure with embedded divertor coils and cryo-pump is presented in section 2. In section 3 the forces acting to the new divertor and coil structure are presented.

The target shaping is discussed in section 4. A summary is given in section 5.

## 2. Conceptual design of the upper divertor

This paper presents the technical concept for the physics driven modification of the upper divertor. The rationale for ‘advanced’ divertor configurations, the set of magnetic configurations, as well as a discussion on target shaping is presented in an own paper [2].

The technical requirements for the divertor design are identified by an iteration process between modelling of ‘advanced’ divertor configurations [2] and the requirements of LSN magnetic configurations (Fig. 1), as well as technical constraints.

The requirements identified for the new upper divertor Div-IIo are:

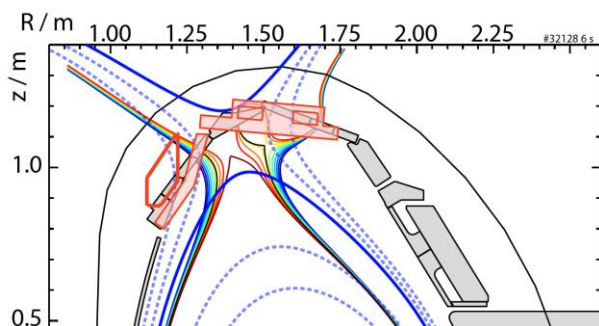
1. Two divertor coils with up to 50 kAt each, allowing to access ‘advanced’ divertor configurations. The coils are separated by about 100 mm. The distance between coils and target surface should be minimized.
2. The coils are operated in both polarities, but with currents in the opposite directions. Parallel and anti-parallel current feeding should be investigated as option.
3. Existing reference discharges in LSN configuration should be compatible with the new structure of the upper divertor.
4. Pumping speed of at least  $S_{\text{eff}} = 15 \text{ m}^3/\text{s}$  in the private flux region to ensure a pumping capability comparable to the existing cryo pump in the lower divertor.
5. Hardening of the upper divertor target structure to cope with the high heating power of AUG for both helicities. This will be achieved by maximizing the target size, minimizing gaps in between targets and moderate shaping at the edges to avoid an overheating near to the gaps.

96 6. The accessibility to the divertor region through  
 97 upper ports for diagnostics should be maximized.

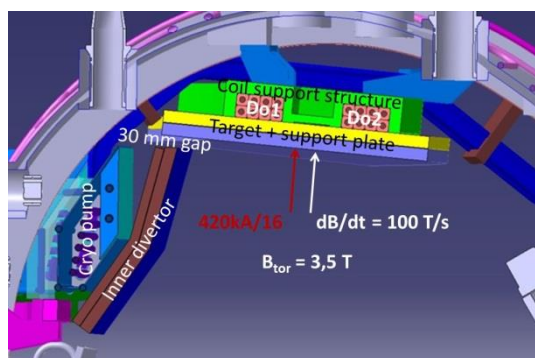
### 98 2.1. Target and coil support structure

99 The present design of the upper divertor is  
 100 optimized for a large plasma volume and there is no  
 101 available space behind the existing divertor to install  
 102 the coils and a cryo pump. Consequently the existing  
 103 divertor structure will be replaced by a new one. The  
 104 plasma facing surface will be moved downwards to  
 105 allow the installation of the coils. However, this is  
 106 limited to  $\Delta z = -100$  mm to be compatible with the  
 107 LSN reference magnetic configuration as shown in Fig.  
 108 1. The coil and the divertor structure are combined in  
 109 the outer divertor to minimize the required space. The  
 110 water cooled divertor support structure acts as the  
 111 cover plate for the coil casing (see Fig. 2). Following  
 112 the ASDEX Upgrade vessel structure - 16 coil and  
 113 divertor support structures will be installed into the 16  
 114 sections of AUG.

115 Electrically, ASDEX Upgrade consists of 8 octants  
 116 connected by a thin 1,2 mm thick stainless steel bellow  
 117 needed for the vacuum tightness. This way the toroidal  
 118 resistance of the AUG vessel is high enough to allow a  
 119 safe discharge break down. Following this concept,  
 120 there is no electrical shortcut over octants by in- or ex-  
 121 vessel components. This has to be considered also for  
 122 the coil support structure that has to be a stiff toroidal  
 123 ring. To avoid a toroidal short cut, the 16 segments of  
 124 the coil support structure will be bolted together with  
 125 screws and isolating SiN ceramic pads.  
 126



127  
 128 Fig. 1 Upper part of AUG with old (gray) and new Div-IIo  
 129 (light red) divertor structure including cryo-pump. The LSN  
 130 reference magnetic configuration is shown in blue. An  
 131 advanced snow flake configuration is shown colored.



132  
 133  
 134 Fig. 2 CAD view of the new Div-IIo,.

### 135 2.2. Divertor coils

136 The 'advanced' divertor configurations require a  
 137 maximum coil current of 50 kAt with a coil separation  
 138 of about 100 mm. The coil will be operated in a quasi  
 139 DC mode with a current ramp rate of max. 15 kA/s.

140 There exist different concepts and technical  
 141 solutions for in-vessel coils. In the conceptual design  
 142 phase we are considering 3 coil concepts.

143 The AUG A-coil conductor that was qualified with  
 144 the company HABIA Cables [3]. The conductor is a  
 145 copper tube with a bore for the water cooling isolated  
 146 by extruded PEEK.

147 Two coil concepts with a water cooled copper  
 148 conductor inside a shielding tube. The isolation  
 149 between the shielding tube and the copper conductor is  
 150 realised by magnesium oxide as for the ITER in vessel  
 151 coils [4, 5], silicon, or polyamide as for the DIII-D in-  
 152 vessel coils [6]. In these concepts, the shielding tube  
 153 acts as vacuum barrier.

154 AUG is operated with pulse lengths of max. 10 s,  
 155 i.e. there is no need for an active cooling that would  
 156 provide constant coil temperature during the discharge.  
 157 Instead the same concept as for all AUG in-vessel  
 158 components will be applied: Adiabatic heating during  
 159 the pulse and recooling afterwards with a typical cool  
 160 down time of a few minutes.

161 The maximum temperature rise of the divertor coil  
 162 at the end of a 5 s long current plateau with 50 kAt is  
 163 set to  $\Delta T = 50$  K for the parameter definition. Using Cu  
 164 as conductor material this defines the maximum current  
 165 density of about 45 A/mm<sup>2</sup>, i.e between 3 kA and 10  
 166 kA coil current for the A-coil and the shielded coil  
 167 concept, respectively. Correspondingly, the number of  
 168 turns/coil becomes 18 (3x6) and 5, respectively.

169 The temperature increase of  $\Delta T = 50$  K of the  
 170 copper conductor will result in a certain stress. A  
 171 detailed FEM calculation will be done for the final coil  
 172 design. Nevertheless first estimations can be done  
 173 assuming that the temperature difference between the  
 174 copper and the stiff surrounding is  $\Delta T = 50$  K. The  
 175 pressure acting on the copper conductor follows to:  
 176  $\frac{F}{A} = \frac{\Delta L}{L} E = \alpha \Delta T E (MPa) \approx 90$  or about or about  
 177 80 % of the yield strength of copper. Here, E is  
 178 Young's modulus and  $\alpha$  the thermal expansion  
 179 coefficient.

180 During the baking the temperature difference  
 181 between components is below  $\Delta T = 10$  K due to the  
 182 slow temperature increase. Stress is induced due to the  
 183 slightly different thermal expansion coefficient of  
 184 copper and stainless steel of about (10%). Due to the  
 185 moderate baking temperature of 150°C at ASDEX  
 186 Upgrade the resulting stress will be lower than during  
 187 coil operation.

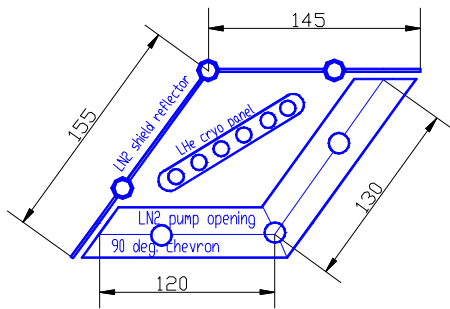
188 The final design on the applied coil concept will be  
 189 taken after prototype tests that are ongoing. Main  
 190 criteria are the electric strength and the handling, inside  
 191 the torus, in particular the bending.

### 192 2.3. Cryo pump

193 A physics program with USN magnetic  
 194 configurations requires a pumping in the upper divertor

195 region to control the neutral pressure. Consequently, a  
 196 cryo pump will be installed together with the new  
 197 divertor structure. The cryo pump in the lower divertor  
 198 [7, 8] has a pumping speed of  $100 \text{ m}^3/\text{s}$ . It is placed at  
 199 major radius of  $R = 2.2 \text{ m}$  and is toroidally distributed  
 200 over about 70% of the toroidal circumference. The  
 201 effective pumping area is given by the  $2.45 \text{ m}^2$  of the  
 202 chevron at liquid nitrogen temperature and  $2.0 \text{ m}^2$  at  
 203 liquid He temperature (about 4 K), see Fig. 3. In the  
 204 upper divertor the cryo pump is placed behind the inner  
 205 divertor at about  $R = 1.2 \text{ m}$  and the effective pumping  
 206 area is reduced. As a consequence the pumping speed  
 207 is lower,  $S_p = 50 \text{ m}^3/\text{s}$ . To guarantee an effective  
 208 pumping speed of  $S_{\text{eff}} = 15 \text{ m}^3/\text{s}$  at the plasma the  
 209 conductance between cryo pump and private flux  
 210 region in the upper divertor has to be higher than  
 211  $25 \text{ m}^3/\text{s}$ . This is realized by the present design. It  
 212 foresees a 30 mm wide slit between the outer and the  
 213 inner divertor plate and the resulting conductance for  
 214 deuterium is  $65 \text{ m}^3/\text{s}$ , well above the required value and  
 215 would result in an effective pumping speed in the  
 216 private flux region of  $S_{\text{eff}} = 28 \text{ m}^3/\text{s}$ .

217 The AUG cryo pump is operate with saturated  
 218 liquid helium. The capacity of the existing He-liquefier  
 219 (18 kg/h) can supply the existing lower (4 g/s) and the  
 220 new upper cryo pump (3 g/s).



221  
 222 Fig. 3 Cross section of the existing AUG cryo-pump.

### 223 3. Forces

224 The AUG vacuum vessel is suspended by 8 rods.  
 225 These suspension rods are fixed at the support structure  
 226 of the toroidal field coils. The total weight of the  
 227 vacuum vessel is about 650 kN, being about half of the  
 228 totally allowed load to the suspension rods of about  
 229 1300 kN. During disruptions, an additional load up to  
 230 450 kN was measured with strain gauges.

231 Access to the vacuum is possible by  $2 \times 3$  small  
 232 vacuum ports (max. 63 mm diameter) pointing up and  
 233 down, respectively and two 280 mm dia. horizontal  
 234 ports in each of the 16 sectors. In addition there are 8  
 235 A-ports and  $2 \times 8$  280 mm dia. B-ports alternating  
 236 between the sectors in the midplane, see Fig. 4.

237 Due to the restricted access through the ports the  
 238 divertor coils have to be fixed inside the vacuum vessel  
 239 and the interaction force between divertor coils and  
 240 external coils has to be taken by the vessel and the  
 241 suspension rods. In the following, first the static forces  
 242 acting in between coils are estimated followed by a  
 243 disruption analysis.

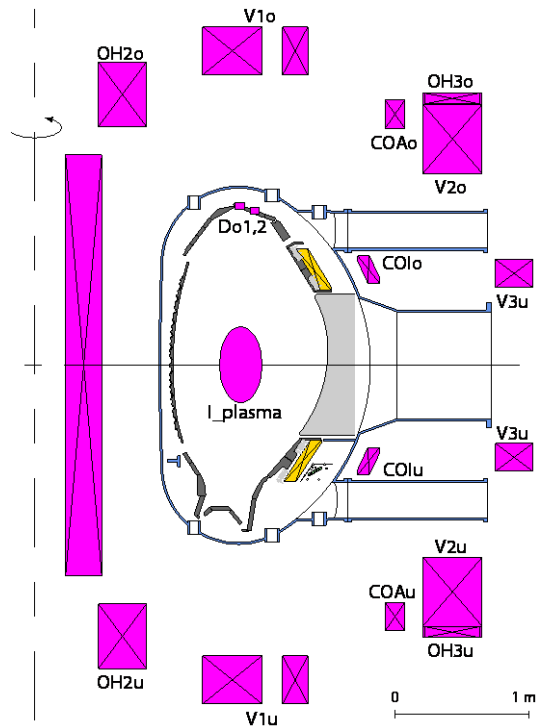
### 244 3.1. Static forces

245 The poloidal field coils are supported by an external  
 246 support structure independently from the toroidal field  
 247 structure and the vacuum vessel. The coils and their  
 248 arrangement around the vacuum vessel are indicated in  
 249 Fig. 4.

250 For an estimation of the static forces onto the vessel  
 251 itself and the suspension rods the worst case of  
 252 maximum currents through the divertor coils and the  
 253 poloidal field coils will be discussed. In reality, the  
 254 supply current is by about a factor of two lower due to  
 255 limitations of the power supply units. For the case that  
 256 both divertor coil currents have the same polarity  
 257 (parallel feeding) the resulting force on the divertor  
 258 coils is  $>640 \text{ kN}$ . This force is in the order of the vessel  
 259 weight of 650 kN. Parallel feeding would lift up the  
 260 vessel or double the weight depending on the polarity.  
 261 This brings us to the conclusion that the parallel  
 262 feeding should not be considered as realistic option  
 263 with the present support structure of the vacuum vessel.

264 The net force to the coil package is reduced for  
 265 anti-parallel feeding to about 12 kN without plasma  
 266 current and is about 16 kN with the maximum applied  
 267 plasma current of  $I_p = 1.4 \text{ MA}$ . This force is below 3%  
 268 of the vessel weight and can be taken by the suspension  
 269 rods. Nevertheless, on a single coil the total force of  
 270  $\pm 640 \text{ kN}$  is applied and a torque remains due to the  
 271 finite distance between the coils of about 100 mm. This  
 272 torque and the force between the coils of about 30 kN  
 273 has to be taken by the coil support structure.

274



275

276 Fig. 4 Cross section of AUG vessel and positions of the  
 277 divertor and poloidal field coils

278 In order to achieve the desired advanced divertor  
 279 configurations, an imbalance of the coil currents is  
 280 required to realize the envisaged magnetic

281 configurations. The case with -52 kAt and 41 kAt  
 282 current in the divertor coils for a realistic plasma  
 283 configuration with  $I_p=1$  MA was calculated with  
 284 ANSYS-FEM. The resulting interaction force to the  
 285 coil is about 17 kN, i.e. equivalent to the worst case  
 286 force estimation for anti-parallel feeding and maximal  
 287 current in the poloidal field coils. The magnetic  
 288 configurations used in the modeling to define the  
 289 physics goals can be realized technically in  
 290 ASDEX Upgrade.

### 291 3.2. Disruption forces

292 Disruptions are a main concern for safe machine  
 293 and diagnostic operation. For the new upper divertor,  
 294 Div-IIo, we will consider:

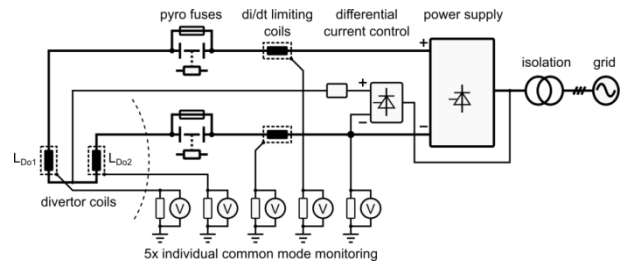
- 295 • Halo currents flowing through the structure towards  
 296 the vessel.
- 297 • Eddy currents induced in the support and divertor  
 298 structure.
- 299 • Voltage and currents induced in the divertor coil.

300 During disruptions, voltages will be induced in the  
 301 support structure and the coils. The coil support  
 302 structure is divided in 16 sub segments which are  
 303 isolated from each other. It could be segmented further  
 304 to reduce eddy and halo currents to a limit tolerable for  
 305 the mechanical structure. For the force estimation it is  
 306 assumed that 30% of the plasma current,  $I_p=1.4$  MA,  
 307 is flowing into the upper divertor structure (Fig. 2). This  
 308 results in about 26 kA/module and about 10 kN force at  
 309 each of the 4 fixing points in case of the maximum  
 310 toroidal field strength of  $B_t = 3.5$  T.

311 The coil and the divertor support structure have  
 312 typical dimensions of about  $300 \times 600 \text{ mm}^2$  and  
 313  $400 \times 600 \text{ mm}^2$ , respectively. For stainless steel and a  
 314  $dB/dt = 100$  T/s the induced torque is 13 kNm and  
 315 22 kNm, respectively. For a single module the torque  
 316 has to be taken by the support at the vessel. With the  
 317 present coil and divertor concept the single modules  
 318 are mechanically connected to a stiff toroidal ring and  
 319 the force of about 100 kN resulting from the torque is  
 320 balanced at the interface between the modules. The  
 321 electric insulation in between modules is realized by  
 322 SiN ceramics that can withstand the high loads.

323 A main concern of the design is the voltage induced  
 324 into the upper coil during disruptions. Due to the large  
 325 area, the induced voltage,  $U_{ind} = -N A \frac{dB}{dt}$ , is 5.4 kV  
 326 and 6.7 kV for the inner and outer coil, respectively.  
 327 For force reasons the coils have to be operated anti-  
 328 parallel. This will be hardwired (Fig. 5) so the induced  
 329 voltage at the coil current feed through is reduced to  
 330 tolerable 1.3 kV. Nevertheless, this high voltage can  
 331 drive a current that is 10-20 times larger than the  
 332 nominal coil current, in case of a low external  
 333 resistance as the power supply is. To avoid such a  
 334 strong current and the resulting forces during a  
 335 disruption, lasting about 10 ms, additional coils  
 336 limiting the current increase,  $dI/dt$ , are added in-  
 337 between the divertor coils and the power supply. They  
 338 limit the current raise during a disruption to about  
 339 0.3 kA. As a further safety measure, pyro fuses can be

341 installed to open the coil circuit. A fail-safe  
 342 unbalancing of the coil current is needed to realize the  
 343 required magnetic configurations. Therefore, an  
 344 additional power supply with passive current limitation  
 345 (output resistors) will be connected to the common  
 346 junction of both divertor coils.



348 Fig. 5 Principal electrical scheme of the power supply and the  
 349 safety elements.  
 350

351 Halo and eddy currents to the divertor and coil  
 352 support structure are in the same order of magnitude as  
 353 in other components of AUG and can be handled.  
 354 Special attention is needed to realize passive safety for  
 355 divertor coil operation.

### 356 4. Target shaping

357 The outer divertor structure will be a well aligned  
 358 stiff ring because it acts also as coil casing. That's why  
 359 there are no gaps and no steps between divertor  
 360 sections. From this, there is no need for module and  
 361 target tilting and flat divertor plates without tilting will  
 362 be installed. This allows operating the divertor with  
 363 both helicities of the magnetic field configurations. A  
 364 sequence of LSN – DN – USN magnetic configuration  
 365 can be run as in the past. By reversing the direction of  
 366 the toroidal magnetic field (helicity) upper USN  
 367 magnetic configurations can be operated with ion-grad  
 368 B drift direction towards the divertor, which is found to  
 369 provide favorable plasma properties.

370 Technically, the assembly tolerance will result in a  
 371 step of  $\pm 0,1$  mm between adjacent target tiles. The  
 372 toroidal gap size will be  $< 1$ mm. Leading edge effects  
 373 are estimated with a simple geometric picture and 5  
 374 deg for the maximum pitch angle between the magnetic  
 375 field line and the flat target surface. With these  
 376 parameters the edge heat load is about 2.5 times the  
 377 heat load at the flat part of the target. In reality the  
 378 temperature increase will be lower due to the  
 379 favourable heat transport into the target at the edges.

380 In addition, we have experimental experiences with  
 381 flat targets and gaps of about 1mm exposed in the  
 382 lower divertor. The experimental results confirm that  
 383 gaps below 1 mm did not result in overheated edges.

384 The clamping concept itself is not finalized yet  
 385 because it depends on the target material which will be  
 386 either tungsten/tungsten alloy or tungsten coated  
 387 graphite. In any case, the clamping concept will allow  
 388 mounting targets with arbitrary shape.

## 389 5. Summary and Conclusions

390 The concept for a new upper divertor in ASDEX  
391 Upgrade with in-vessel coils to investigate ‘advanced’  
392 magnetic configurations is presented. ‘Advanced’  
393 magnetic configurations are part of a risk mitigation  
394 strategy should the conventional divertor configuration  
395 approach not be applicable for future fusion reactors.  
396 The new upper divertor, Div-IIo; consists of an outer  
397 divertor with embedded divertor coils, an inner divertor  
398 and a cryo pump with 15 m<sup>3</sup>/s effective pumping speed  
399 in the private flux region. The new divertor coils will  
400 be design for 50 kAt and can be operated for 5s plateau  
401 phase. Halo and eddy currents flowing through the  
402 divertor and coil support structure are in the same order  
403 of magnitude as in other components of AUG and can  
404 be handled. Special attention is needed to realize  
405 passive safety for divertor coil operation. The flat  
406 arrangement of the target tiles allows operation with  
407 both helicities of the magnetic configuration.

## 408 409 References

- 410 [1] A. Herrmann, (Guest editor), Special Issue on ASDEX  
411 Upgrade, Fusion Science and Technology, 44 (2003) 1-  
412 747.
- 413 [2] T. Lunt, A. Kallenbach, H. Zohm, A. Herrmann, M.  
414 Wischmeier, Y. Feng, A.U. team, Design of an  
415 alternative upper divertor in ASDEX Upgrade supported  
416 by EMC3-Eirene simulations, Nuclear Materials and  
417 Energy (PSI2016), submitted for publication (2016).
- 418 [3] I. Zammuto, M. Rott, B. Streibl, W. Suttrop, T. Vierle,  
419 Conceptual design of in vessel mid-plane saddle coils for  
420 fast AC operation in ASDEX Upgrade, Fusion Eng.  
421 Des., 86 (2011) 1067- 1071.
- 422 [4] M. Kalish, P. Heitzenroeder, A. Brooks, L. Bryant, J.  
423 Chrzanowski, E. Daly, R. Feder, J. Feng, M. Messineo,  
424 M. Gomez, C. Hause, T. Bohm, I. Griffiths, A. Lipski,  
425 M. Mardenfeld, M. Nakahira, C. Neumeyer, R.  
426 Pillsbury, M. Sawan, M. Schaffer, R. Simmons, P. Titus,  
427 I. Zatz, T. Meighan, Iter In-Vessel Coil design and  
428 R&D, in: 2011 IEEE/NPSS 24th Symposium on  
429 Fusion Engineering, 2011, pp. 1-6.
- 430 [5] A. Encheva, H.Omran, A.Devred, A.Vostner, N.Mitchell,  
431 F.L. CH.Jun, C.Zhou, B.Macklin, HP.Marti, C.Sborchia,  
432 A.DellaCorte, A.Dizenobio, A.Anemona, H.J. Y.Wu,  
433 A.Xu, J.Jin, Progress on the Design Development and  
434 Prototype Manufacturing of the ITER In-Vessel Coils,  
435 Fusion Eng. Des., SOFT 2016 (2016).
- 436 [6] P.M. Anderson, C.B. Baxi, A.G. Kellman, E.E. Reis,  
437 Design, fabrication, installation, testing and initial  
438 results of in-vessel control coils for DIII-D, in: 20th  
439 IEEE/NPSS Symposium onFusion Engineering, 2003.,  
440 2003, pp. 573-576.
- 441 [7] B. Streibl, S. Deschka, O. Gruber, B. Jüttner, P. Lang, K.  
442 Mattes, G. Pautasso, J. Perchermeier, K. Schippl, H.  
443 Schneider, U. Seidel, W. Suttrop, G. Teller, M.  
444 Weissgerber, In-Vessel Cryo Pump for ASDEX Upgrade  
445 Divertor II, in: C. Varandas, F. Serra (Eds.) Fusion  
446 Technology (Proc. of the 19th Symposium on Fusion  
447 Technology, Lisbon, 1997), Elsevier, Amsterdam, 1997,  
448 pp. 427-430.
- 449 [8] B. Streibl, A. Kaltenberger, H. Kollotzek, K. Mattes, V.  
450 Rohde, G. Schall, K. Schindler, Operational behaviour  
451 of the ASDEX upgrade in-vessel cryo pump, Fusion  
452 Eng. Des., 56-7 (2001) 867-872.
- 453